

## Article

# Influence of Wind Flows on Surface O<sub>3</sub> Variation over a Coastal Province in Southeast China

Yukun Shen <sup>1</sup>, Jane Liu <sup>1,2</sup> , Zhixiong Chen <sup>1,\*</sup>, Mengmiao Yang <sup>1</sup> , Lei Shu <sup>1</sup> , Chende Gai <sup>1</sup>  
and Yongcheng Jiang <sup>3</sup>

<sup>1</sup> Key Laboratory for Humid Subtropical Eco-Geographical Processes of the Ministry of Education, School of Geographical Sciences, Fujian Normal University, Fuzhou 350117, China

<sup>2</sup> Department of Geography and Planning, University of Toronto, Toronto, ON M5S 3G3, Canada

<sup>3</sup> Xiamen Key Laboratory of Straits Meteorology, Xiamen Meteorological Bureau, Xiamen 361000, China

\* Correspondence: zchen@fjnu.edu.cn

**Abstract:** Surface ozone (O<sub>3</sub>) is influenced not only by anthropogenic emissions but also by meteorological factors, with wind direction being one of the most overlooked factors. Here, we combine the observational data of both O<sub>3</sub> and wind flow to compare the variation in surface O<sub>3</sub> with wind direction between coastal and inland regions of Fujian, a province in the southeast coast of China with complicated topography. We further conduct a numerical simulation using a global chemical transport model, GEOS-Chem, to interpret the observational results, explore the linkages between these O<sub>3</sub> variations and wind flows, and identify the dominant processes for the occurrence of high O<sub>3</sub> that varies with wind flows. The results from the observations over 2015–2021 suggest that, over coastal regions, surface O<sub>3</sub> concentrations show a strong dependence on wind flow changes. On average, during the daytime, when southeasterly winds prevail, the mean of O<sub>3</sub> concentrations reaches 83.5 µg/m<sup>3</sup>, which is 5.0 µg/m<sup>3</sup> higher than its baseline values (the mean O<sub>3</sub> concentrations), while the northwesterly winds tend to reduce surface O<sub>3</sub> by 6.4 µg/m<sup>3</sup>. The positive O<sub>3</sub> anomalies with southeasterly wind are higher in the autumn and summer than in the spring and winter. During the nighttime, the onshore northeasterly winds are associated with enhanced O<sub>3</sub> levels, likely due to the air mass containing less NO<sub>2</sub>, alleviating the titration effects. Over inland regions, however, surface O<sub>3</sub> variations are less sensitive to wind flow changes. The GEOS-Chem simulations show that the prevailing southeasterly and southwesterly winds lead to the positive anomaly of chemical reactions of O<sub>3</sub> over coastal regions, suggesting enhanced photochemical production rates. Furthermore, southeasterly winds also aid in transporting more O<sub>3</sub> from the outer regions into the coastal regions of Fujian, which jointly results in elevated surface O<sub>3</sub> when southeasterly winds dominates. When affected by wind flows in different directions, the chemical reaction and transport in the inland regions do not exhibit significant differences regarding their impact on O<sub>3</sub>. This could be one of the reasons for the difference in O<sub>3</sub> distribution between coastal and inland regions. This study could help to deepen our understanding of O<sub>3</sub> pollution and aid in providing an effective warning of high-O<sub>3</sub> episodes.

**Keywords:** O<sub>3</sub> concentration; southeast China; wind flow



**Citation:** Shen, Y.; Liu, J.; Chen, Z.; Yang, M.; Shu, L.; Gai, C.; Jiang, Y. Influence of Wind Flows on Surface O<sub>3</sub> Variation over a Coastal Province in Southeast China. *Atmosphere* **2024**, *15*, 262. <https://doi.org/10.3390/atmos15030262>

Academic Editor: Giacomo Alessandro Gerosa

Received: 5 January 2024

Revised: 18 February 2024

Accepted: 19 February 2024

Published: 22 February 2024



**Copyright:** © 2024 by the authors. Licensee MDPI, Basel, Switzerland. This article is an open access article distributed under the terms and conditions of the Creative Commons Attribution (CC BY) license (<https://creativecommons.org/licenses/by/4.0/>).

## 1. Introduction

Tropospheric ozone (O<sub>3</sub>) is photochemically produced from its precursors such as VOC and NO<sub>x</sub> in the presence of solar radiation, and has great impacts on human health, the ecosystem, and the climate [1–3]. Due to the high level of anthropogenic emissions, surface O<sub>3</sub> concentrations over China have continuously increased in recent years. The summertime mean maximum 8 h average (MDA8) O<sub>3</sub> was observed to have increased at a rate of 1.9 ppbv per year since 2013 [4]. More than 90% of Chinese urban monitoring sites showed an increasing O<sub>3</sub> trend, and 30% of them even increased at a rate of 3.0 ppbv per

year [5]. As a result, the worsening O<sub>3</sub> conditions have become an emerging problem for air quality in China.

In addition to the anthropogenic emissions of O<sub>3</sub> precursors, the variation in surface O<sub>3</sub> concentrations is also controlled by meteorological processes, which are often the direct causes of severe pollution episodes [6,7]. Meteorology can not only determine the environmental conditions for O<sub>3</sub> chemical reactions, but also influence the emissions of natural biogenic VOCs serving as O<sub>3</sub> precursors [8]. Moreover, meteorology also controls the transport of O<sub>3</sub> and its precursors from region to region [9–12]. Many studies have found that synoptic conditions with strong solar radiation, high temperature, low moisture, and weak winds are conducive to the formation and accumulation of O<sub>3</sub> [13–15]. Among the meteorological factors, winds are crucial for the synoptic evolution influencing both chemical reactions and the transport processes of O<sub>3</sub>. For example, the meso-scale systems, such as mountain–valley wind and sea breeze, are important triggers for convective cloud development, which can significantly alter the availability of solar radiation and the variations in temperature and humidity, and hence change the production rate of O<sub>3</sub> [16–18]. The local winds also influence the supply of precursors and the transport processes of O<sub>3</sub>. While weak winds help with O<sub>3</sub> accumulation, strong winds can effectively transport high levels of O<sub>3</sub> and its precursors to downstream regions [19]. At a larger scale, the wind circulation, temperature, humidity, and cloud conditions basically follow the evolution of synoptic-scale weather systems, which determines the seasonal O<sub>3</sub> variation. It has been found that surface O<sub>3</sub> is positively correlated with the intensity of the East Asian summer monsoon (EASM). The horizontal wind flow and vertical wind structure associated with strong and weak EASM in different years directly changes the formation of O<sub>3</sub> [20–22]. Therefore, investigations of the role of meteorology, such as wind flows in high O<sub>3</sub> episodes, are warranted in order to gain a complete understanding of O<sub>3</sub> pollution.

Numerous studies have been performed over the most rapidly developing areas in China, such as the North China Plain (NCP), Yangtze River Delta (YRD), and the Pearl River Delta (PRD), confronting severe O<sub>3</sub> pollution [23–26]. The lessons learned from these regions can effectively inspire O<sub>3</sub> mitigation policies for other areas and deserve extra consideration given the increasing O<sub>3</sub> found over many parts of China. Taking Fujian province as an example, it is located in the eastern edge of East Asia, which is directly impacted by the subtropical high, typhoons, and the subtropical jet stream [27–29]. The complicated topographical distribution of Fujian is characterized by alternating coasts, narrow plains, and mountainous regions just within 300 km. As a result, local winds such as mountain–valley wind and sea breeze often occur [30,31]. In terms of emissions, large cities distributed over coastal and plain regions contribute to high anthropogenic emissions, while the inland mountainous regions with a high forest cover fraction are rich in BVOC emissions. Moreover, Fujian is located between the PRD and YRD. Provided with winds at small or large scales, Fujian is susceptible to O<sub>3</sub> pollution transported from outer regions such as PRD and YRD, and hence becomes a crossroads for O<sub>3</sub>-polluted airmass. It is found that 24–38% of O<sub>3</sub> pollution episodes over Fujian are caused by the regional transport of high levels of O<sub>3</sub> from outer regions [32], though there are also strong variations in its internal emission variations from coastal to inland regions. In brief, O<sub>3</sub> in Fujian is modulated by both external (such as EASM and O<sub>3</sub> regional transport) and internal factors (local emissions and meso-scale weather systems), leading to a coast–inland contrast between O<sub>3</sub> distributions. In view of previous studies, wind direction is likely to be an influential factor on surface O<sub>3</sub> variations in Fujian, but also one of the most overlooked factors. Therefore, this study is focused on investigating how wind direction impacts surface O<sub>3</sub> levels in coastal and inland areas of Fujian, and how an enhanced understanding of those impacts can aid in developing effective warning systems for high-O<sub>3</sub> episodes. Through the analysis of O<sub>3</sub> variations with wind direction, we aim to elucidate the driving role of wind direction in O<sub>3</sub> pollution against the background of different emission levels, different weather conditions, and different geographical factors. Based on simulations from a chemical transport model, GEOS-Chem, we identify the dominant processes that

modulate the occurrence of high O<sub>3</sub> concentrations varying with wind flow. The results from this study not only provide a foundation for a deeper understanding of O<sub>3</sub> pollution but also serve as a crucial reference and basis for future O<sub>3</sub> pollution warnings.

## 2. Data and Methods

### 2.1. Surface Air Pollutant Measurements and Meteorological Observations

Surface O<sub>3</sub> measurements from 43 sites distributed over 9 cities in Fujian during 2015–2021 were analyzed in this study (Figure 1). Surface O<sub>3</sub> and NO<sub>2</sub> data were obtained from the National Environmental Monitoring General Station of China (<http://www.cnemc.cn/>, last access: 5 September 2023). Surface O<sub>3</sub> concentrations were measured using an ultraviolet spectrophotometric ozone analyzer (Thermo Model 49i), while NO<sub>2</sub> concentrations were measured using an analyzer based on chemiluminescence (Thermo Model 42i). The temporal resolution of measurements is 1 h. According to the geolocations, we divided all the sites into coastal regions, including Ningde (ND), Fuzhou (FZ), Putian (PT), Quanzhou (QZ), Xiamen (XM), and Zhangzhou (ZZ), and the inland regions, including Nanping (NP), Sanming (SM), and Longyan (LY). Figure 1 shows the distribution of these regions, along with the topography of Fujian. Coastal regions are mainly located in plain areas, while the inland regions are distributed over mountainous regions. Taking the coastline as a reference, the distance from the inland stations to the coastline ranges from 108 to 170 km, while the distance from the coastal stations ranges from 0.9 to 30 km.

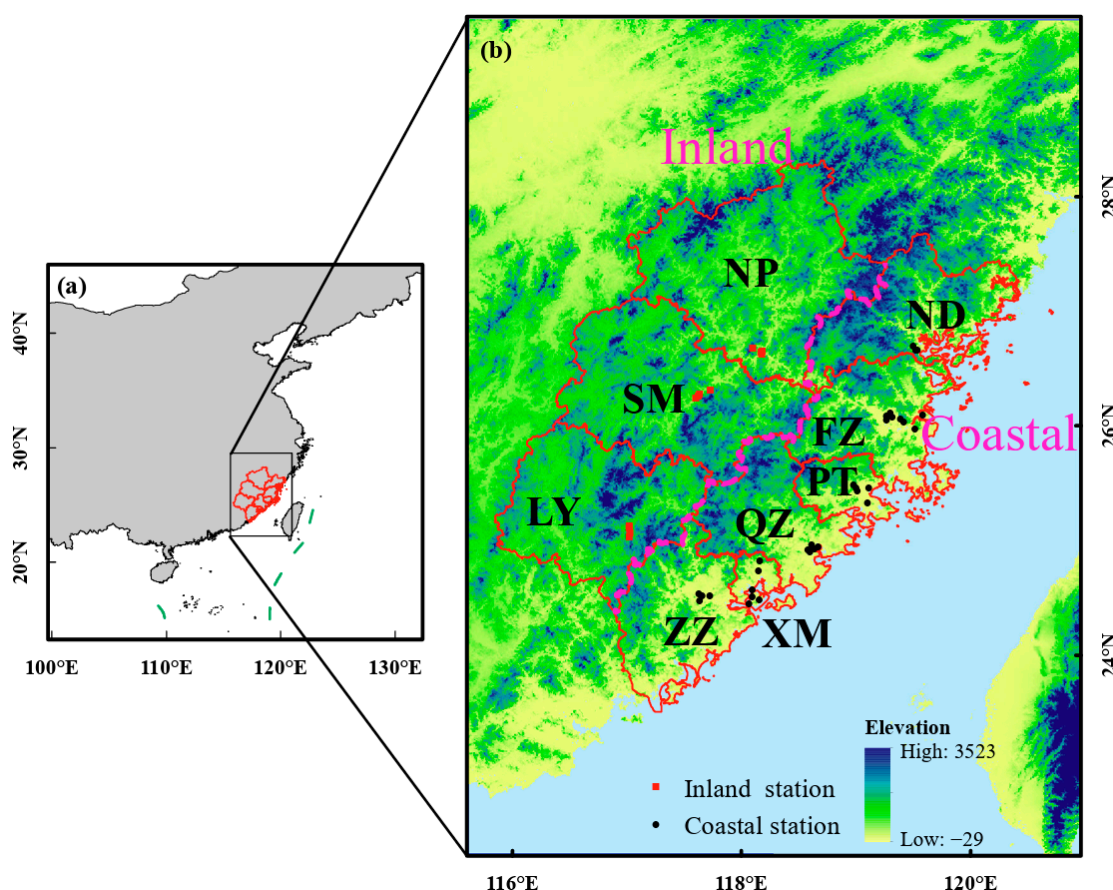


**Figure 1.** Geolocation of Fujian province (a) and topography of Fujian (b). The nine city districts, enclosed by red outlines, are divided into coastal (Ningde (ND), Fuzhou (FZ), Putian (PT), Quanzhou (QZ), Xiamen (XM), and Zhangzhou (ZZ)) and inland (Nanping (NP), Sanming (SM), and Longyan (LY)) regions in this study. The 43 surface air pollutant measurement sites are indicated by the black (coastal) and red (inland) dots.

Surface meteorological observations include temperature, wind direction, wind speed, relative humidity (RH), and precipitation with 1 h temporal resolution. The data were obtained from the Fujian Meteorological Bureau. Generally, air quality stations and meteorological stations are not in exactly the same location. Therefore, we matched air quality data with the meteorological data from the closest possible station. According to the wind directions with a spacing of  $10^\circ$ , the concurrent air pollutant and meteorological data were paired for each hour. The seasonal average of  $O_3$  concentrations at a given hour over all wind directions was treated as the baseline ( $\overline{O_3}$ ). For example, the  $O_3$  concentrations at 10:00, averaged from June to August in 2017 at a given station, would be the  $O_3$  baseline at 10:00 in summer 2017 for that station. The departure of  $O_3$  concentrations in a given direction from the baseline in the season was treated as an anomaly ( $\Delta O_3$ ):

$$\Delta O_3 = O_{3,i} - \overline{O_3} \quad (i = 0, 10^\circ \dots 360^\circ \text{ for wind direction}) \quad (1)$$

Therefore, we isolated the impact of wind direct on surface  $O_3$ , by removing seasonal and diurnal  $O_3$  variations in the background.

In addition to surface observations, we also acquired gridded wind data from the National Aeronautics and Space Administration (NASA) Modern-Era Retrospective analysis for Research and Applications, version 2 (MERRA-2) [33]. MERRA-2 data were used to explore the linkage between wind flow and  $O_3$  concentrations simulated by GEOS-Chem. The horizontal resolution of MERRA-2 is  $0.5^\circ \times 0.625^\circ$ , the number of vertical layers is 72, and the temporal resolution is 3 h. MERRA-2 is a long-term global reanalysis produced by the NASA Global Modeling and Assimilation Office (GMAO). The data reflect recent advances in atmospheric modeling and data assimilation. Equation (1) was applied for both observational and MERRA-2 wind data.

## 2.2. GEOS-Chem Model

To explore the dominant processes responsible for  $O_3$  variations over Fujian, associated with different wind flows, we conducted numerical simulations using the GEOS-Chem model (v12.9.3; <http://geos-chem.org>, last access: 15 January 2023)

GEOS-Chem [34] is a global chemical transport model driven by gridded meteorological data. It currently uses MERRA-2 reanalysis data as a default, which was also the case in this study. GEOS-Chem has been widely applied in atmospheric chemistry, air quality, and climate change studies [9,12,13,21,29,35–37]. The GEOS-Chem's full chemistry simulation includes fully coupled  $O_3$ –NO<sub>x</sub>–VOC–halogen–aerosol chemistry. We conducted the full chemistry simulation using the non-local planetary boundary layer mixing scheme [38]. The horizontal resolution was  $0.5^\circ \times 0.625^\circ$  over eastern China, with chemical boundary conditions archived every 3 h from global simulations with  $2^\circ \times 2.5^\circ$  resolution. Emissions were configured using the Harvard–NASA Emission Component (HEMCO) [39]. Biogenic VOC emissions, including isoprene, monoterpenes, and sesquiterpenes, were calculated online using the Model of Emissions of Gases and Aerosols from Nature (MEGAN v2.1; [40]). Soil NO<sub>x</sub> emissions were calculated based on the available nitrogen (N) in soils and edaphic conditions such as soil temperature and moisture [41]. Global default anthropogenic emissions were from the Community Emissions Data System (CEDS [42]). Open fire emissions were from the Global Fire Emissions Database (GFED4 [43]).

The budget diagnosis was defined as the  $O_3$  mass change in grid cells in the planetary boundary layer (PBL) column due to different processes, including chemistry, horizontal transport, vertical transport, mixing, and deposition [44]. In this study, we define the net chemical production as the C-term, the horizontal transport as the T-term, and the sum of the three terms in the vertical direction as the CMD term, which includes convection (vertical transport), mixing, and deposition. These terms can be output directly from GEOS-Chem's full chemistry simulation.

### 3. Results

#### 3.1. Overview of O<sub>3</sub> Distribution in Fujian

Based on the observational data, the seasonal variation and diurnal cycle of surface O<sub>3</sub> in coastal and inland regions of Fujian during 2015–2021 were compared (Figures 2 and 3). Generally, O<sub>3</sub> concentrations in coastal cities are higher than those in inland cities. The mean of O<sub>3</sub> concentrations in coastal cities is 62.7 μg/m<sup>3</sup>, which is 37.5% higher than that in inland cities (45.6 μg/m<sup>3</sup>). This difference between the two regions is because coastal regions have stronger anthropogenic emissions favoring O<sub>3</sub> generation, less vegetated areas for O<sub>3</sub> removal, and more inflowing O<sub>3</sub> transported from the outside [32]. These factors collectively contribute to the difference in O<sub>3</sub> variations between coastal and inland areas.

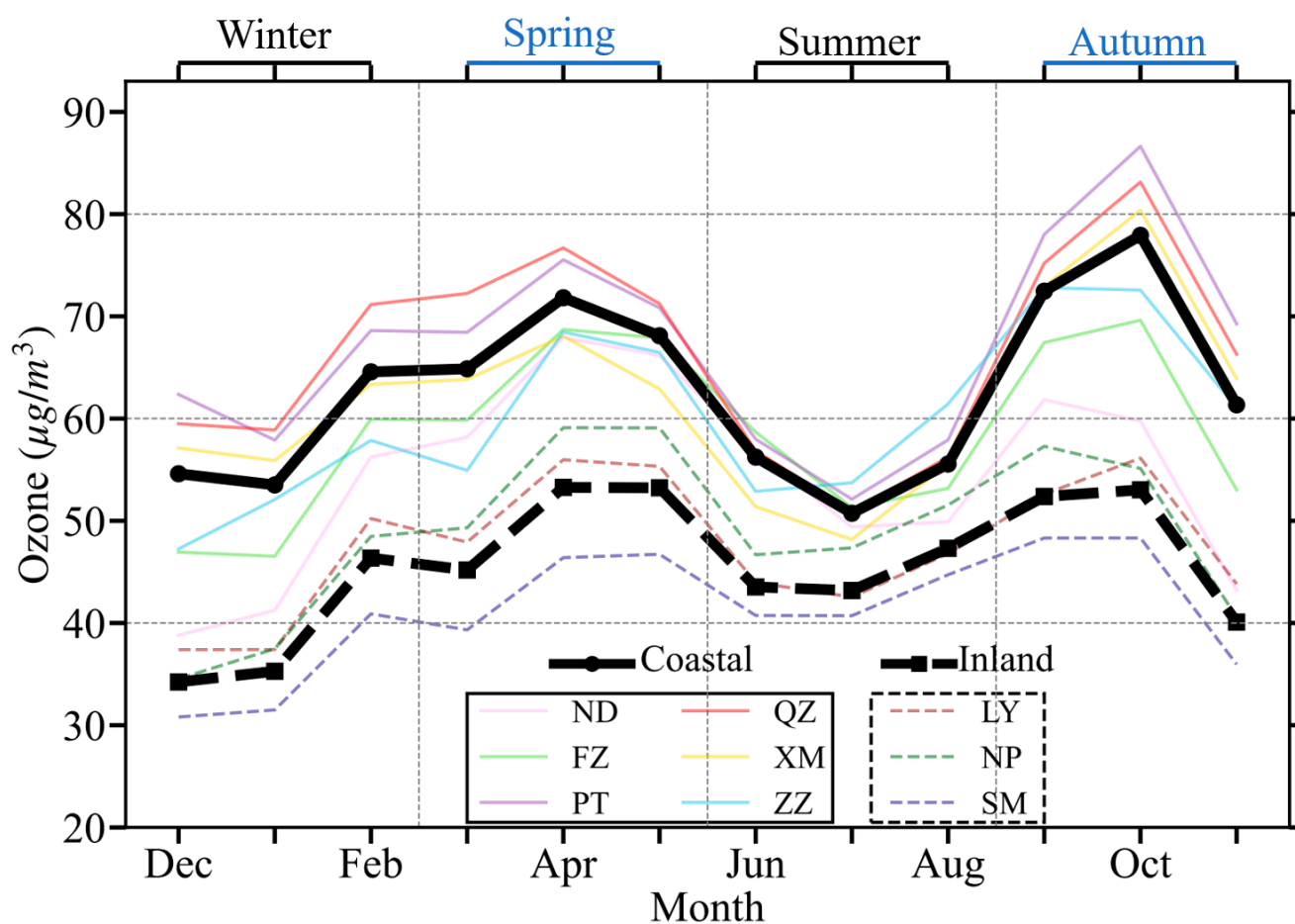


**Figure 2.** Monthly variations in surface O<sub>3</sub> concentrations (unit: μg/m<sup>3</sup>) in Fujian, averaged over coastal cities (thick solid black line), including Ningde (ND), Fuzhou (FZ), Putian (PT), Quanzhou (QZ), Xiamen (XM), and Zhangzhou (ZZ), and inland cities (thick dashed black line), including Nanping (NP), Sanming (SM), and Longyan (LY). Solid and dashed thin lines indicate coastal and inland cities, respectively. The O<sub>3</sub> concentrations are the mean over 2015–2021, based on observational data.

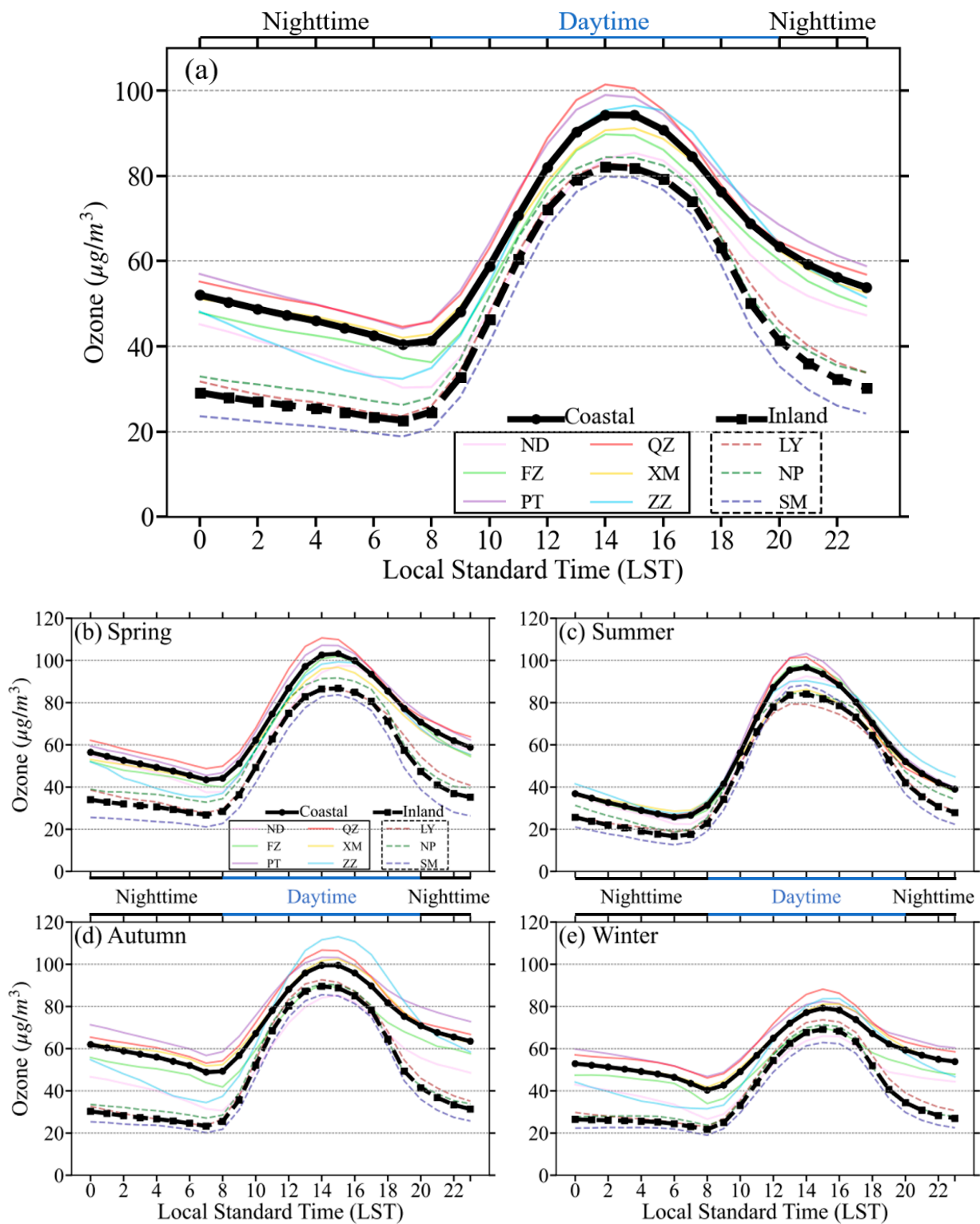


**Figure 3.** (a) Diurnal cycle of surface O<sub>3</sub> concentrations (unit: µg/m<sup>3</sup>) in coastal cities (thick solid black line) and inland cities (thick dashed black line) during 2015–2021 in Fujian. (b–e) show the diurnal cycle in spring (b), summer (c), autumn (d), and winter (e). Coastal cities include Ningde (ND), Fuzhou (FZ), Putian (PT), Quanzhou (QZ), Xiamen (XM), and Zhangzhou (ZZ), while inland cities include Nanping (NP), Sanming (SM), and Longyan (LY). The O<sub>3</sub> concentrations are the mean over 2015–2021 based on observational data.

The seasonality of  $O_3$  in coastal and inland cities is the same, with two peaks in the spring and autumn and two valleys in the summer and winter. The difference in  $O_3$  concentrations between coastal and inland cities also varies with season. The maximum difference occurs in October, reaching  $24.9 \mu\text{g}/\text{m}^3$ , and this is greatly reduced in summer, with a minimum in July ( $7.6 \mu\text{g}/\text{m}^3$ ). Meteorology, especially radiation, is one of the primary modulators of seasonal  $O_3$  variations. High radiation levels, high air temperature, and low air humidity tend to enhance the surface  $O_3$  levels. In Fujian, the summer is characterized by frequent rainfall, and rainy weather is often associated with cloudy conditions and reduced solar radiation, leading to lower  $O_3$  concentrations. In the winter, lower temperatures result in a slowdown of photochemical reaction rates, leading to decreased  $O_3$  concentrations.

The diurnal cycle of  $O_3$  in Fujian shows a peak at 14:00 local standard time (LST) and a valley at 07:00 LST. The maximum  $O_3$  concentrations in coastal and inland cities are  $94.3 \mu\text{g}/\text{m}^3$  and  $82.2 \mu\text{g}/\text{m}^3$ , respectively, while the minimum concentrations are  $40.5 \mu\text{g}/\text{m}^3$  and  $22.6 \mu\text{g}/\text{m}^3$ , respectively. Over the course of a day, the  $O_3$  level in coastal cities is consistently higher than that in inland cities. The difference in the diurnal cycle of  $O_3$  in coastal and inland cities is more significant during the nighttime (20:00–08:00 LST). The difference also varies over different seasons; the difference is largest in autumn, but smallest in summer.

### 3.2. Influence of Wind Flows on Surface $O_3$

The wind flows are affected by various factors, including topography, land and ocean proximity, and atmospheric circulations. Consequently, wind flows differ strongly in coastal and inland cities in Fujian, as shown in the observational data (Figure 4). In the spring (Figure 4a,e), northeasterly and southeasterly winds prevail in coastal cities, while southwesterly winds dominate in inland cities. In the summer (Figure 4b,f), the dominant winds are southerly in coastal cities and southwesterly in inland cities. During the autumn (Figure 4c,g) and winter (Figure 4d,h), northeasterly winds prevail in both coastal and inland cities.

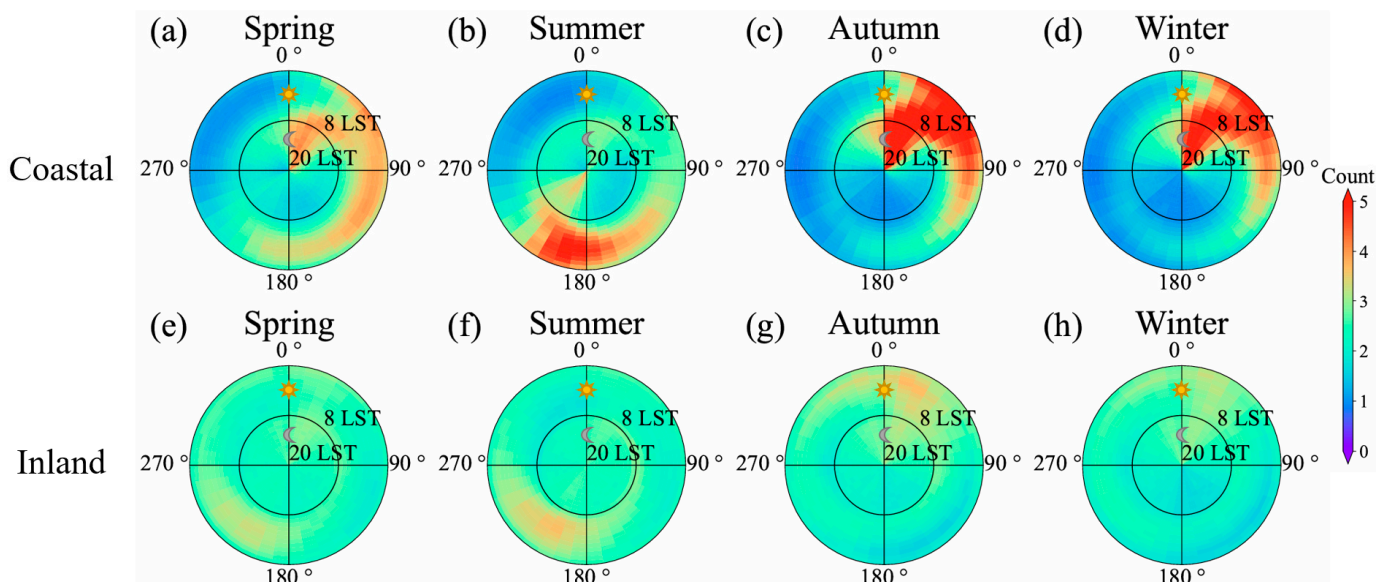


**Figure 4.** Variations in hourly surface wind direction in coastal (a–d) and inland (e–h) cities of Fujian by season. The color indicates the occurrences of wind direction per season at an interval of  $10^\circ$  over each hour, ranging from low (in blue) to high (in red). The inner rings represent the nighttime, from 20:00 to 08:00 (LST), and the outer rings represent the daytime, from 08:00 to 20:00 (LST). The value of the count is the mean over 2015–2021 based on the observational data.

Provided with concurrent wind flow and O<sub>3</sub> observations, we calculated the mean O<sub>3</sub> concentrations for different wind directions each hour for coastal (Figure 5a–d) and inland (Figure 5e–h) cities, respectively. Compared with inland cities, surface O<sub>3</sub> concentrations in coastal cities are higher, especially in the daytime, during the spring and autumn. In the same season, O<sub>3</sub> varies more significantly with wind direction over coastal cities than over inland cities. Over coastal cities, surface O<sub>3</sub> under northeasterly and southeasterly winds is obviously higher than under northwesterly and southwesterly winds. Over inland cities, O<sub>3</sub> concentrations are more uniform under different wind directions, showing a weaker influence of wind flow on O<sub>3</sub> variations.

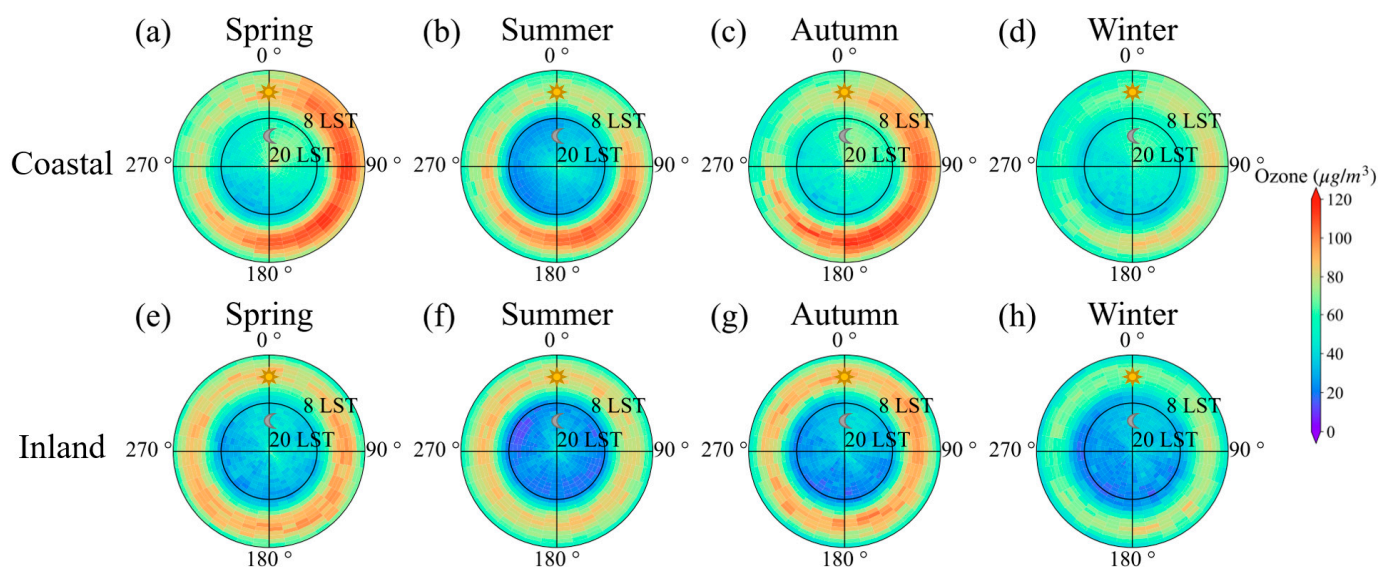


**Figure 5.** Hourly O<sub>3</sub> concentrations (unit:  $\mu\text{g}/\text{m}^3$ ) by wind direction in coastal (a–d) and inland (e–h) cities of Fujian over four seasons. The inner rings represent the nighttime, from 20:00 to 08:00 (LST), and the outer rings represent the daytime, from 08:00 to 20:00 (LST). The value of O<sub>3</sub> concentrations is the mean over 2015–2021 based on observational data.

To further reveal the extent to which wind flows influence surface O<sub>3</sub> variations, we compared the hourly O<sub>3</sub> anomaly ( $\Delta\text{O}_3$ ) under each wind direction with to the corresponding seasonal O<sub>3</sub> mean in all directions in the same hour (the baseline; see Equation (1)) (Figure 6). In coastal cities (Figure 6a–d), it is obvious that the easterly winds usually enhance O<sub>3</sub> concentrations, while the westerly winds generally reduce O<sub>3</sub>. This strong contrast in O<sub>3</sub> concentrations between the easterly and westerly wind flows appears in all seasons. In the daytime, the onshore winds, especially southeasterly winds, can, on average, increase surface O<sub>3</sub> in coastal cities by up to  $15 \mu\text{g}/\text{m}^3$  above the corresponding seasonal mean in the same hour. During the nighttime, when O<sub>3</sub> photochemical reactions are absent, it is clear that O<sub>3</sub> is enhanced by the onshore northeasterly winds.

We quantitatively compared O<sub>3</sub> concentrations and key environmental parameters such as temperature, RH, and precipitation under different wind directions in coastal and inland cities (Table 1). In coastal cities, during the daytime, temperature is generally higher and RH is lower under southeasterly winds than under the other wind directions; these two conditions are conducive to O<sub>3</sub> photochemical production, while southwesterly and northwesterly winds tend to trigger convective clouds, hindering the availability of solar radiation for O<sub>3</sub> production. As a result, O<sub>3</sub> concentrations under southeasterly winds reach  $83.5 \mu\text{g}/\text{m}^3$ , which is  $5.0 \mu\text{g}/\text{m}^3$  higher than the baseline value. During the nighttime, the onshore northeasterly winds contain less NO<sub>2</sub>, which is  $3.0 \mu\text{g}/\text{m}^3$  lower than its baseline value (Table 2). The reduced NO<sub>2</sub> concentrations effectively alleviate the titration of O<sub>3</sub>, and hence lead to enhanced nighttime O<sub>3</sub> concentrations when northeasterly winds prevail.

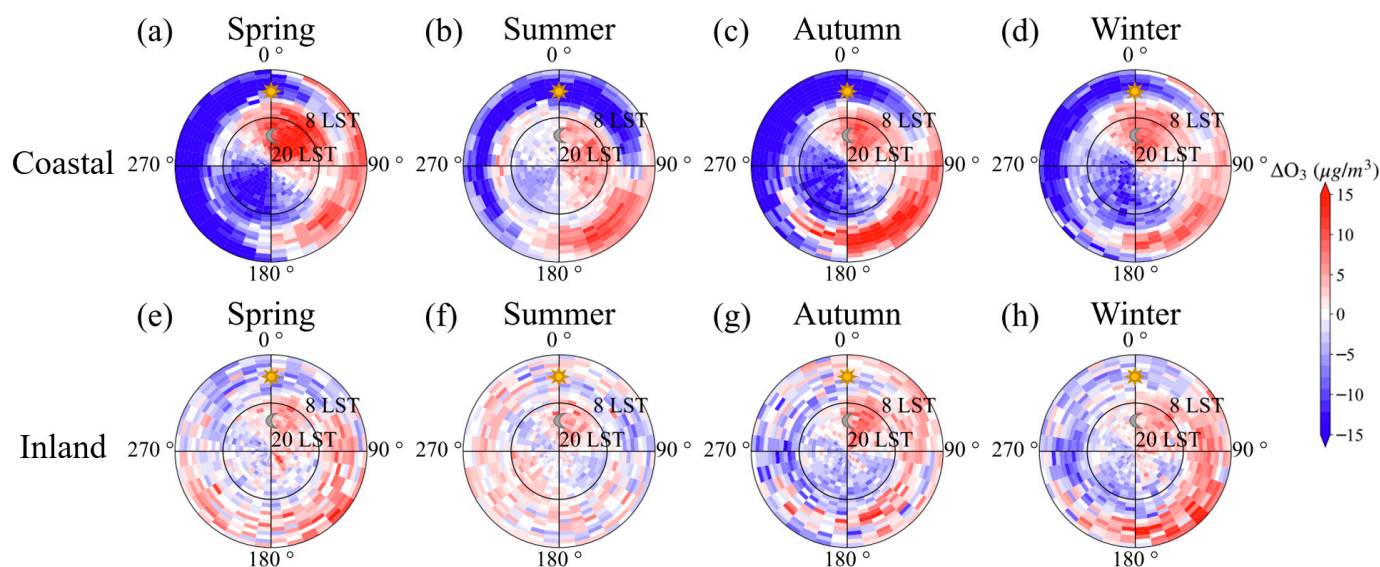


**Figure 6.** The same as Figure 5, but for O<sub>3</sub> anomalies (see Equation (1)). (a–d): coastal cities. (e–h): inland cities. The value of O<sub>3</sub> concentrations is the mean over 2015–2021 based on observational data.

**Table 1.** Mean O<sub>3</sub>, O<sub>3</sub> anomalies ( $\Delta O_3$ ), temperature, RH, and precipitation under different wind directions during the daytime (08:00–20:00 LST) in coastal and inland cities in Fujian. The values are the means over 2015–2021 based on observational data.

Wind Direction	O <sub>3</sub> ( $\mu\text{g}/\text{m}^3$ )		$\Delta O_3$ ( $\mu\text{g}/\text{m}^3$ )		T ( $^{\circ}\text{C}$ )		RH (%)		Precipitation (mm/h)	
	Coastal	Inland	Coastal	Inland	Coastal	Inland	Coastal	Inland	Coastal	Inland
Northeasterly ( $0^{\circ}$ – $90^{\circ}$ )	78.1	64.9	0.4	0.7	21.8	21.5	66.0	67.2	0.2	0.2
Southeasterly ( $90^{\circ}$ – $180^{\circ}$ )	83.5	65.7	5.0	2.2	24.7	24.3	69.5	66.2	0.1	0.2
Southwesterly ( $180^{\circ}$ – $270^{\circ}$ )	67.4	64.8	−4.8	−0.1	26.1	25.1	71.0	65.3	0.2	0.2
Northwesterly ( $270^{\circ}$ – $360^{\circ}$ )	57.9	62.2	−6.4	−1.8	21.7	22.2	71.6	67.2	0.3	0.3

**Table 2.** Mean O<sub>3</sub>, O<sub>3</sub> anomalies ( $\Delta O_3$ ), NO<sub>2</sub>, and NO<sub>2</sub> anomalies ( $\Delta \text{NO}_2$ ) under different wind directions during the nighttime (20:00–08:00 LST) in coastal and inland cities in Fujian. The values are the means over 2015–2021 based on observational data.

Wind Direction	O <sub>3</sub> ( $\mu\text{g}/\text{m}^3$ )		$\Delta O_3$ ( $\mu\text{g}/\text{m}^3$ )		NO <sub>2</sub> ( $\mu\text{g}/\text{m}^3$ )		$\Delta \text{NO}_2$ ( $\mu\text{g}/\text{m}^3$ )	
	Coastal	Inland	Coastal	Inland	Coastal	Inland	Coastal	Inland
Northeasterly ( $0^{\circ}$ – $90^{\circ}$ )	62.8	37.5	6.6	3.7	18.1	18.3	−3.0	−2.3
Southeasterly ( $90^{\circ}$ – $180^{\circ}$ )	51.5	32.3	0.4	−0.6	21.1	23.0	−0.5	1.7
Southwesterly ( $180^{\circ}$ – $270^{\circ}$ )	38.7	29.8	−8.4	−1.5	24.2	22.6	2.8	0.7
Northwesterly ( $270^{\circ}$ – $360^{\circ}$ )	47.4	32.6	−1.4	−1.1	22.5	21.6	1.4	−0.1

Regarding the prevailing wind, O<sub>3</sub> concentrations vary with season, region, and time of day (Figures 4–6). Taking the daytime as an example, in spring, the prevailing winds in coastal regions are southeasterly and northeasterly, which are associated with O<sub>3</sub> concentrations of 88.0  $\mu\text{g}/\text{m}^3$  and 88.6  $\mu\text{g}/\text{m}^3$ , respectively, leading to the most positive O<sub>3</sub> anomalies among all wind directions; in inland regions, under the prevailing southwest winds, O<sub>3</sub> concentrations are 71.5  $\mu\text{g}/\text{m}^3$ , resulting in the second most positive O<sub>3</sub> anomalies among all wind directions. In summer, the prevailing winds in both coastal and inland areas are southwesterly, leading to O<sub>3</sub> concentrations of 69.0  $\mu\text{g}/\text{m}^3$  and 67.6  $\mu\text{g}/\text{m}^3$ , respectively, signaling a minor negative (positive) O<sub>3</sub> anomaly in coastal (inland) regions. In the autumn and winter, the prevailing winds in both coastal and inland regions are northeasterly, resulting in O<sub>3</sub> concentrations in coastal regions of 82.9  $\mu\text{g}/\text{m}^3$  and 66.5  $\mu\text{g}/\text{m}^3$ , respectively, while in inland regions, the concentrations are 71.7  $\mu\text{g}/\text{m}^3$  and 54.8  $\mu\text{g}/\text{m}^3$ , respectively. In coastal regions, O<sub>3</sub> concentrations under the prevailing wind rank the second highest

among all wind directions in both the autumn and winter, while in inland regions,  $O_3$  concentrations under the prevailing wind rank first in autumn, and second in winter.

### 3.3. Source Attribution of $O_3$ Variations Associated with Different Wind Flows

Surface  $O_3$  variations are controlled by photochemical reactions, transport, mixing, and deposition processes. Under the influence of different wind flows, the environmental conditions and dispersion of  $O_3$  differ, and thus lead to  $O_3$  variations. To reveal the dominant processes responsible for the  $O_3$  variations associated with different wind flows, we used GEOS-Chem simulations to interpret the contribution of different processes (C-term, T-term, and CMD-term) to  $O_3$  variations in the surface layer, with reference to the wind flows.

The simulated  $O_3$  from the GEOS-Chem model is shown in Figure 7. Compared with the observations (Figure 5), the model can reproduce the higher  $O_3$  levels in coastal cities compared to inland cities. The large variation in  $O_3$  in coastal cities with different wind flows is also captured. While  $O_3$  concentrations in inland cities are overestimated to some extent, the model performs reasonably well in simulating  $O_3$  in coastal cities.

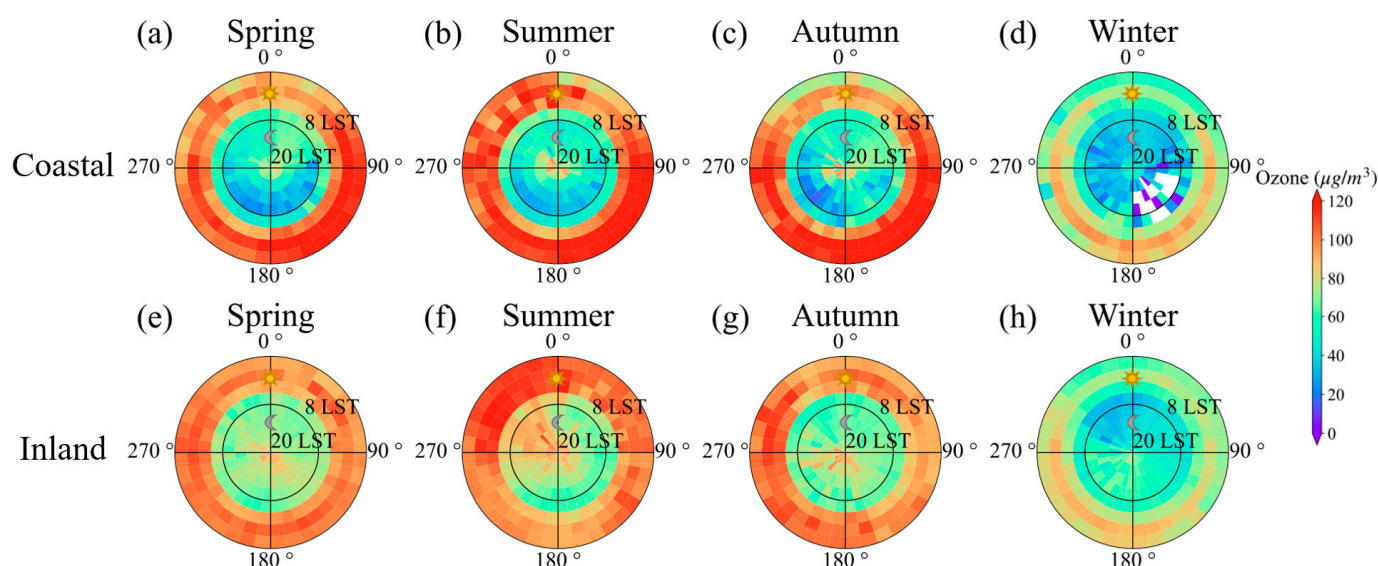


**Figure 7.** The same as Figure 5, but for simulated  $O_3$  concentrations from GEOS-Chem simulations for coastal cities (a–d) and inland cities (e–h). To be consistent with GEOS-Chem simulations, wind data from MERRA-2 are used. All data are taken from the corresponding grids in GEOS-Chem and MERRA-2 data for the coastal and inland cities.

Given the pronounced dependence of  $O_3$  on wind flows, we calculated the contributions of C-term (net chemical production), T-term (horizontal transport), and CMD-term (convection, mixing, and deposition) to the total  $O_3$  budget based on GEOS-Chem simulations under different wind flows (Figure 8 and Tables 3 and 4). When southeasterly and southwesterly winds prevail over coastal cities during the daytime (Table 3), the dominant process responsible for  $O_3$  variations is chemical reaction (C-term) (Figure 8b,c), leading to an enhanced production rate above the baseline levels, and, hence, higher concentrations (Figure 7a–d). In contrast, northeasterly and northwesterly winds tend to reduce the C-term, leading to weakened, photochemically produced  $O_3$  (Figure 8a,d). Specifically, under the influence of southeasterly wind, the total  $O_3$  budget anomaly can be maximized, with a value of  $0.39 \text{ kg/s}$ , compared with its baseline value. The positive total  $O_3$  budget directly results in a positive  $O_3$  anomaly of  $5.57 \mu\text{g}/\text{m}^3$ , in good agreement with the observed value ( $5.0 \mu\text{g}/\text{m}^3$ ). In terms of horizontal  $O_3$  transport (T-term), onshore winds, including northeasterly and southeasterly winds, tend to transport high- $O_3$  air mass into the coastal regions, as seen in the positive anomaly of T-term (Figure 8e,f), while the prevailing southwesterly

and northwesterly winds show a negative T-term anomaly (Figure 8g,h), suggesting that the winds are conducive to transporting cleaner air. The  $\Delta$ CMD-term generally ranges between  $\pm 0.15$  kg/s, and is smaller than the C-term and T-term under all wind directions, except under southeasterly winds, when the term has a negative impact on the ozone anomaly. Based on the above analysis, we found that the prevailing southeasterly winds can enhance the chemical production and bring in high-O<sub>3</sub> air, resulting in higher O<sub>3</sub> levels than under the other wind directions in coastal regions of Fujian.

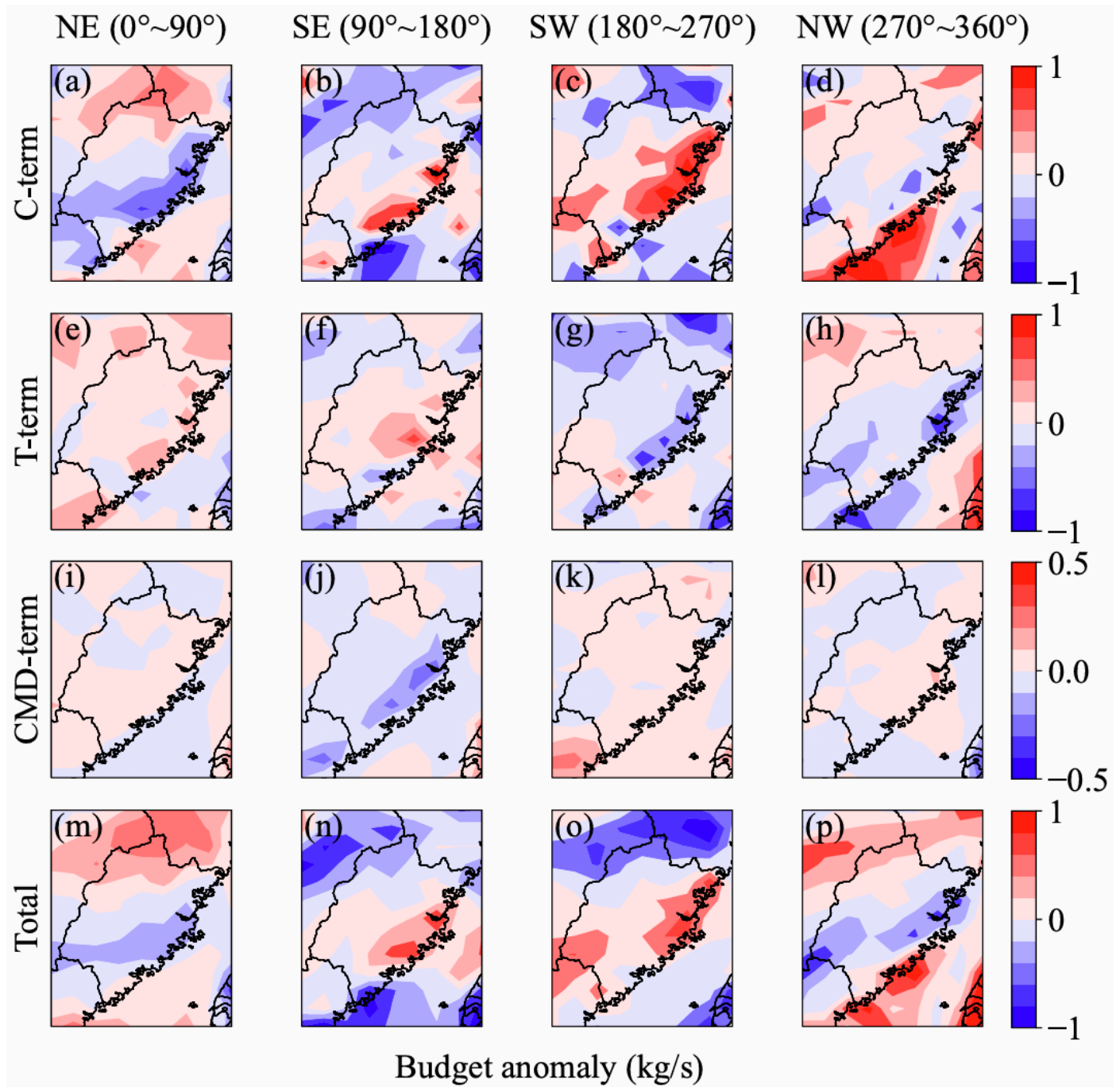


**Figure 8.** The anomaly of the contributions of C-term (net chemical production) (a–d), T-term (horizontal transport) (e–h), and CMD-term (convection, mixing, and deposition) (i–l) to the total O<sub>3</sub> budget (m–p) relative to their baseline values (unit: kg/s) in Fujian. The values are the means during the daytime (08:00–20:00 LST) based on GEOS-Chem simulations.

**Table 3.** Mean anomaly of the total O<sub>3</sub> budget, O<sub>3</sub> concentrations, C term (net chemical production), T term (horizontal transport), and CMD term (convection, mixing, and deposition), with respect to wind direction during the daytime (08:00–20:00 LST) in coastal regions in Fujian, based on GEOS-Chem simulations.

Wind Direction	$\Delta$ Total O <sub>3</sub> Budget (kg/s)	$\Delta$ O <sub>3</sub> ( $\mu\text{g}/\text{m}^3$ )	$\Delta$ C-Term (kg/s)	$\Delta$ T-Term (kg/s)	$\Delta$ CMD-Term (kg/s)
Northeasterly (0°–90°)	−0.23	−0.79	−0.43	0.17	0.02
Southeasterly (90°–180°)	0.39	5.57	0.46	0.08	−0.15
Southwesterly (180°–270°)	0.32	−1.3	0.57	−0.29	0.04
Northwesterly (270°–360°)	−0.23	−0.76	−0.04	−0.24	0.04

**Table 4.** The same as Table 3, but for the nighttime (20:00–08:00 LST).

Wind Direction	$\Delta$ Total O <sub>3</sub> Budget (kg/s)	$\Delta$ O <sub>3</sub> ( $\mu\text{g}/\text{m}^3$ )	$\Delta$ C-Term (kg/s)	$\Delta$ T-Term (kg/s)	$\Delta$ CMD-Term (kg/s)
Northeasterly (0°–90°)	0.07	1.69	−0.02	0.08	0.01
Southeasterly (90°–180°)	−0.23	0.50	−0.06	−0.13	−0.04
Southwesterly (180°–270°)	−0.07	−4.47	0.05	−0.17	0.05
Northwesterly (270°–360°)	0.03	−0.66	0.06	0.07	−0.10

In our previous study [32], we also found that the inflow of O<sub>3</sub> to Fujian from outer regions is mainly transported from the north along the east coast of China, mostly from highly polluted areas in YRD, and then from the sea to the land across the coastline in Fujian by easterly, northeasterly, or southeasterly winds. The transport pathways also vary with season. O<sub>3</sub> transport from YRD is strong in the spring and autumn, weak in the summer, and almost zero in the winter. Some O<sub>3</sub> is also transported from the PRD, which is strongest in spring. This study used a Eulerian approach with GEOS-Chem to track air movement, while Ge et al. [32] used a backward trajectory analysis, similar to others [45–47]; both studies achieved consistent results.

The contributions of the three terms to the nighttime O<sub>3</sub> variations were also analyzed (Table 4). The surface measurements suggest that, in the coastal regions, the northeasterly winds transport air mass containing less NO<sub>2</sub>, and thus reduces the titration of O<sub>3</sub> (Table 2). Referring to the simulations, despite the small anomalies in the chemical production and the CMD terms (Table 4), GEOS-Chem suggests that O<sub>3</sub> transport facilitated by northeasterly wind plays an important role in enhancing nighttime O<sub>3</sub>.

#### 4. Conclusions

Meteorological environments play an important role in determining surface O<sub>3</sub> variations. Among the meteorological factors, wind flows can significantly change the evolution of synoptic processes, and hence influence the crucial environmental conditions for O<sub>3</sub> chemical reactions, horizontal and vertical transport, mixing, and deposition. This study analyzes the concurrent surface O<sub>3</sub> and meteorological observations over 2015–2021 to untangle the influence of wind flow on surface O<sub>3</sub> variations in Fujian, a coastal province in southeast China, with complicated topography and different levels of O<sub>3</sub> precursor emissions between coastal and inland regions. Furthermore, Fujian is also a crossroad for O<sub>3</sub>-polluted air mass due to its geolocation between the YRD and the PRD. Therefore, under the influence of different wind flows, it is worth examining the responses of surface O<sub>3</sub> to wind and investigate the dominant processes responsible for O<sub>3</sub> variations. The main conclusions as follows:

- (1) Under different emission conditions and topography distributions, the mean of O<sub>3</sub> concentrations over 2015–2021 is 62.7  $\mu\text{g}/\text{m}^3$  in coastal regions of Fujian, where anthropogenic emissions are higher, while it is 45.6  $\mu\text{g}/\text{m}^3$  in inland mountainous regions with higher forest coverage. Seasonally, O<sub>3</sub> concentrations show peaks in the

spring and autumn and valleys in the summer and winter, as seen in both coastal and inland regions (Figure 1). Throughout the year, the O<sub>3</sub> level is also higher in coastal regions than in inland regions; the difference in O<sub>3</sub> concentrations between coastal and inland regions also shows distinct seasonality, with a maximum in October, reaching 24.9 µg/m<sup>3</sup>, and a minimum of 7.6 µg/m<sup>3</sup> in July.

- (2) Surface O<sub>3</sub> over coastal regions shows a strong dependence on wind flow changes (Figures 5 and 6; Tables 1 and 2). When southeasterly winds prevail over coastal regions, the mean of surface O<sub>3</sub> concentrations in the daytime reaches 83.5 µg/m<sup>3</sup>, which is 5.0 µg/m<sup>3</sup> higher than its baseline value, while northwesterly winds tend to reduce surface O<sub>3</sub> by 6.4 µg/m<sup>3</sup>. The positive anomaly in O<sub>3</sub> associated with southeasterly winds is higher in the autumn and summer than in the spring and winter. During the nighttime, the onshore northeasterly winds are associated with enhanced O<sub>3</sub> levels since the air mass contains less NO<sub>2</sub>, alleviating the titration effects, as well as the enhanced transport of O<sub>3</sub>. Over inland regions, however, surface O<sub>3</sub> variations are less sensitive to wind flow changes.
- (3) The GEOS-Chem model was applied to diagnose the dominant processes for surface O<sub>3</sub> variations associated with different wind flows (Figure 8; Tables 3 and 4). High-resolution simulations reasonably capture the observed variations in O<sub>3</sub> in terms of day–night contrast, coast–inland region contrast, and, especially, contrasts under different wind flows. The simulation results show that the prevailing southeasterly and southwesterly winds lead to a positive anomaly in O<sub>3</sub> chemical reactions, suggesting enhanced photochemical production rates. Furthermore, southeasterly winds also transport more O<sub>3</sub> from the outer regions into the coastal regions of Fujian, which jointly results in elevated surface O<sub>3</sub> when southeasterly winds dominate.

This study shows some similarities and differences compared with previous studies. For example, surface O<sub>3</sub> in an inland city, Hefei, in China, was found to not be sensitive to variations in wind direction, which is similar to the results obtained in this study, while in a coastal city, Shanghai, surface O<sub>3</sub> is the highest under northwesterly winds in spring [48], rather than under southeasterly winds observed in this study, suggesting a regional dependence of the relationship between surface O<sub>3</sub> and wind direction.

Based on this study, we can make the following recommendations. First, when southeast winds are prevalent, it is advisable to enhance the monitoring of O<sub>3</sub> concentrations in the central and southern coastal regions and implement corresponding control measures. Therefore, establishing a wind direction monitoring network to monitor real-time changes in wind flow in coastal areas is necessary. Second, when northeast or southeast winds are prevalent, attention should be paid to O<sub>3</sub> levels in upstream and downstream source areas, with timely warnings issued for potential O<sub>3</sub> transport events. We also should regularly update the wind direction monitoring results to adjust emission standards under different wind conditions, with a particular emphasis on industrial emission sources during periods of southeast winds, implement more stringent industrial emission control measures during these periods, and integrate meteorological forecasts and wind direction monitoring into the O<sub>3</sub> warning system to establish a more accurate predictive model for high-O<sub>3</sub> events.

The research results of this study are subject to some uncertainties and limitations. For example, O<sub>3</sub> and wind measurements contain certain instrumental errors. The air-quality stations and the nearest meteorological stations are generally not in the same location, but 10–10<sup>3</sup> m apart. Although the model performs reasonably well, GEOS-Chem tends to overestimate O<sub>3</sub> concentrations in the daytime and in inland regions. This study suggests that the higher O<sub>3</sub> observed in the daytime over coastal regions is generally associated with southeasterly wind, due to the higher temperature and lower humidity, which are conducive to O<sub>3</sub> production. However, the chemical reactions that are involved are not specified, and could be a subject for future studies.

Our results emphasize the prominent dependence of surface O<sub>3</sub> variations on wind flow changes over coastal regions of Fujian. Such knowledge could deepen our understanding of O<sub>3</sub> pollution and aid in providing an effective warning for high-O<sub>3</sub> episodes. For other

coastal regions experiencing prominent wind changes due to a combined influence of synoptic weather, sea–land distribution, and local microclimate, these findings can also provide extra insights into O<sub>3</sub> variations with wind. Still, be mindful that surface O<sub>3</sub> responses to wind flow can be regionally dependent.

**Author Contributions:** Conceptualization, Z.C. and J.L.; methodology, Y.S.; validation, J.L. and Z.C.; formal analysis, Y.S. and Z.C.; investigation, Z.C. and J.L.; data curation, Y.S., C.G. and Y.J.; writing—original draft preparation, J.L., Y.S. and Z.C.; writing—review and editing, Z.C. and J.L.; visualization, J.L. and L.S.; supervision, J.L. and Z.C.; funding acquisition, M.Y. and Z.C. All authors have read and agreed to the published version of the manuscript.

**Funding:** This work was supported by the National Natural Science Foundation of China (Grant No. 42105079).

**Institutional Review Board Statement:** Not applicable.

**Informed Consent Statement:** Not applicable.

**Data Availability Statement:** The MREEA-2 reanalysis data analyzed in this study are publicly available and can be found here: <https://gmao.gsfc.nasa.gov/reanalysis/MERRA-2>, accessed on 18 February 2024. Hourly ground-based measurements of surface gaseous pollutant concentrations including O<sub>3</sub> were obtained from the public website of the Chinese Ministry of Ecology and Environment (MEE) (<https://english.mee.gov.cn/>, accessed on 18 February 2024). The meteorological data and GEOS-Chem model simulations presented in this study are available on request from the corresponding author.

**Acknowledgments:** The computing resources used in this study were provided by Fujian Normal University High Performance Computation Center (FNU-HPCC). We thank the Chinese Ministry of Ecology and Environment for the nationwide air pollutant observations, the NASA GMAO for the MERRA-2 reanalysis data and the Harvard University for the GEOS-Chem model. We are grateful to three anonymous reviewers for their constructive comments and suggestions, which helped to improve the quality of this paper.

**Conflicts of Interest:** The authors declare no conflicts of interest.

## References

1. Jacob, D.J.; Winner, D.A. Effect of climate change on air quality. *Atmos. Environ.* **2009**, *43*, 51–63. [CrossRef]
2. Bell, M.L.; Goldberg, R.; Hogrefe, C.; Kinney, P.L.; Knowlton, K.; Lynn, B.; Rosenthal, J.; Rosenzweig, C.; Patz, J.A. Climate change, ambient ozone, and health in 50 US cities. *Clim. Chang.* **2007**, *82*, 61–76. [CrossRef]
3. Shindell, D.; Kuylenstierna, J.C.; Vignati, E.; van Dingenen, R.; Amann, M.; Klimont, Z.; Anenberg, S.C.; Muller, N.; Janssens-Maenhout, G.; Raes, F. Simultaneously mitigating near-term climate change and improving human health and food security. *Science* **2012**, *335*, 183–189. [CrossRef]
4. Li, K.; Jacob, D.J.; Shen, L.; Lu, X.; De Smedt, I.; Liao, H. Increases in surface ozone pollution in China from 2013 to 2019: Anthropogenic and meteorological influences. *Atmos. Chem. Phys.* **2020**, *20*, 11423–11433. [CrossRef]
5. Lu, X.; Zhang, L.; Wang, X.; Gao, M.; Li, K.; Zhang, Y.; Yue, X.; Zhang, Y. Rapid increases in warm-season surface ozone and resulting health impact in China since 2013. *Environ. Sci. Technol. Lett.* **2020**, *7*, 240–247. [CrossRef]
6. Liu, P.; Song, H.; Wang, T.; Wang, F.; Li, X.; Miao, C.; Zhao, H. Effects of meteorological conditions and anthropogenic precursors on ground-level ozone concentrations in Chinese cities. *Environ. Pollut.* **2020**, *262*, 114366. [CrossRef] [PubMed]
7. Lu, X.; Zhang, L.; Shen, L. Meteorology and climate influences on tropospheric ozone: A review of natural sources, chemistry, and transport patterns. *Curr. Pollut. Rep.* **2019**, *5*, 238–260. [CrossRef]
8. Dewan, S.; Lakhani, A. Tropospheric ozone and its natural precursors impacted by climatic changes in emission and dynamics. *Front. Environ. Sci.* **2022**, *10*, 2499. [CrossRef]
9. Gong, C.; Liao, H.; Zhang, L.; Yue, X.; Dang, R.; Yang, Y. Persistent ozone pollution episodes in North China exacerbated by regional transport. *Environ. Pollut.* **2020**, *265*, 115056. [CrossRef]
10. Liu, J.; Wang, L.; Li, M.; Liao, Z.; Sun, Y.; Song, T.; Gao, W.; Wang, Y.; Li, Y.; Ji, D. Quantifying the impact of synoptic circulation patterns on ozone variability in northern China from April to October 2013–2017. *Atmos. Chem. Phys.* **2019**, *19*, 14477–14492. [CrossRef]
11. Lu, X.; Zhang, L.; Chen, Y.; Zhou, M.; Zheng, B.; Li, K.; Liu, Y.; Lin, J.; Fu, T.-M.; Zhang, Q. Exploring 2016–2017 surface ozone pollution over China: Source contributions and meteorological influences. *Atmos. Chem. Phys.* **2019**, *19*, 8339–8361. [CrossRef]
12. Shen, L.; Liu, J.; Zhao, T.; Xu, X.; Han, H.; Wang, H.; Shu, Z. Atmospheric transport drives regional interactions of ozone pollution in China. *Sci. Total Environ.* **2022**, *830*, 154634. [CrossRef] [PubMed]

13. Dang, R.; Liao, H.; Fu, Y. Quantifying the anthropogenic and meteorological influences on summertime surface ozone in China over 2012–2017. *Sci. Total Environ.* **2021**, *754*, 142394. [[CrossRef](#)] [[PubMed](#)]
14. Han, H.; Liu, J.; Shu, L.; Wang, T.; Yuan, H. Local and synoptic meteorological influences on daily variability in summertime surface ozone in eastern China. *Atmos. Chem. Phys.* **2020**, *20*, 203–222. [[CrossRef](#)]
15. Liu, Y.; Wang, T. Worsening urban ozone pollution in China from 2013 to 2017—Part 1: The complex and varying roles of meteorology. *Atmos. Chem. Phys.* **2020**, *20*, 6305–6321. [[CrossRef](#)]
16. Bei, N.; Zhao, L.; Wu, J.; Li, X.; Feng, T.; Li, G. Impacts of sea-land and mountain-valley circulations on the air pollution in Beijing-Tianjin-Hebei (BTH): A case study. *Environ. Pollut.* **2018**, *234*, 429–438. [[CrossRef](#)]
17. Dong, Q.; Zhao, P.; Wang, Y.; Miao, S.; Gao, J. Impact of mountain-valley wind circulation on typical cases of air pollution in Beijing. *Huan Jing Ke Xue* **2017**, *38*, 2218–2230.
18. Wentworth, G.; Murphy, J.; Sills, D. Impact of lake breezes on ozone and nitrogen oxides in the Greater Toronto Area. *Atmos. Environ.* **2015**, *109*, 52–60. [[CrossRef](#)]
19. Xu, J.; Huang, X.; Wang, N.; Li, Y.; Ding, A. Understanding ozone pollution in the Yangtze River Delta of eastern China from the perspective of diurnal cycles. *Sci. Total Environ.* **2021**, *752*, 141928. [[CrossRef](#)]
20. Li, S.; Wang, T.; Huang, X.; Pu, X.; Li, M.; Chen, P.; Yang, X.Q.; Wang, M. Impact of East Asian summer monsoon on surface ozone pattern in China. *J. Geophys. Res. Atmos.* **2018**, *123*, 1401–1411. [[CrossRef](#)]
21. Yang, Y.; Liao, H.; Li, J. Impacts of the East Asian summer monsoon on interannual variations of summertime surface-layer ozone concentrations over China. *Atmos. Chem. Phys.* **2014**, *14*, 6867–6879. [[CrossRef](#)]
22. Zhou, D.; Ding, A.; Mao, H.; Fu, C.; Wang, T.; Chan, L.; Ding, K.; Zhang, Y.; Liu, J.; Lu, A. Impacts of the East Asian monsoon on lower tropospheric ozone over coastal South China. *Environ. Res. Lett.* **2013**, *8*, 044011. [[CrossRef](#)]
23. Hu, J.; Li, Y.; Zhao, T.; Liu, J.; Hu, X.-M.; Liu, D.; Jiang, Y.; Xu, J.; Chang, L. An important mechanism of regional O<sub>3</sub> transport for summer smog over the Yangtze River Delta in eastern China. *Atmos. Chem. Phys.* **2018**, *18*, 16239–16251. [[CrossRef](#)]
24. Shu, L.; Wang, T.; Han, H.; Xie, M.; Chen, P.; Li, M.; Wu, H. Summertime ozone pollution in the Yangtze River Delta of eastern China during 2013–2017: Synoptic impacts and source apportionment. *Environ. Pollut.* **2020**, *257*, 113631. [[CrossRef](#)] [[PubMed](#)]
25. Sun, L.; Xue, L.; Wang, Y.; Li, L.; Lin, J.; Ni, R.; Yan, Y.; Chen, L.; Li, J.; Zhang, Q. Impacts of meteorology and emissions on summertime surface ozone increases over central eastern China between 2003 and 2015. *Atmos. Chem. Phys.* **2019**, *19*, 1455–1469. [[CrossRef](#)]
26. Wang, H.; Lyu, X.; Guo, H.; Wang, Y.; Zou, S.; Ling, Z.; Wang, X.; Jiang, F.; Zeren, Y.; Pan, W. Ozone pollution around a coastal region of South China Sea: Interaction between marine and continental air. *Atmos. Chem. Phys.* **2018**, *18*, 4277–4295. [[CrossRef](#)]
27. Feng, X.; Li, M.; Li, Y.; Yu, F.; Yang, D.; Gao, G.; Xu, L.; Yin, B. Typhoon storm surge in the southeast Chinese mainland modulated by ENSO. *Sci. Rep.* **2021**, *11*, 10137. [[CrossRef](#)] [[PubMed](#)]
28. Herzschuh, U.; Cao, X.; Laepple, T.; Dallmeyer, A.; Telford, R.J.; Ni, J.; Chen, F.; Kong, Z.; Liu, G.; Liu, K.-B. Position and orientation of the westerly jet determined Holocene rainfall patterns in China. *Nat. Commun.* **2019**, *10*, 2376. [[CrossRef](#)] [[PubMed](#)]
29. Jiang, Z.; Li, J.; Lu, X.; Gong, C.; Zhang, L.; Liao, H. Impact of western Pacific subtropical high on ozone pollution over eastern China. *Atmos. Chem. Phys.* **2021**, *21*, 2601–2613. [[CrossRef](#)]
30. Li, Y.; Wang, Y.; Lin, Y.; Fei, R.; Gao, J. Effects of terrain and landmass near Fujian Province of China on the structure and propagation of a long-lived rainband in Typhoon Longwang (2005): A numerical study. *J. Geophys. Res. Atmos.* **2020**, *125*, e2020JD033393. [[CrossRef](#)]
31. Luo, T.; Zhang, T.; Wang, Z.; Gan, Y. Driving forces of landscape fragmentation due to urban transportation networks: Lessons from Fujian, China. *J. Urban Plan. Dev.* **2016**, *142*, 04015013. [[CrossRef](#)]
32. Ge, C.; Liu, J.; Cheng, X.; Fang, K.; Chen, Z.; Chen, Z.; Hu, J.; Jiang, D.; Shen, L.; Yang, M. Impact of regional transport on high ozone episodes in southeast coastal regions of China. *Atmos. Pollut. Res.* **2022**, *13*, 101497. [[CrossRef](#)]
33. Gelaro, R.; McCarty, W.; Suárez, M.J.; Todling, R.; Molod, A.; Takacs, L.; Randles, C.A.; Darmenov, A.; Bosilovich, M.G.; Reichle, R. The modern-era retrospective analysis for research and applications, version 2 (MERRA-2). *J. Clim.* **2017**, *30*, 5419–5454. [[CrossRef](#)]
34. Bey, I.; Jacob, D.J.; Yantosca, R.M.; Logan, J.A.; Field, B.D.; Fiore, A.M.; Li, Q.; Liu, H.Y.; Mickley, L.J.; Schultz, M.G. Global modeling of tropospheric chemistry with assimilated meteorology: Model description and evaluation. *J. Geophys. Res. Atmos.* **2001**, *106*, 23073–23095. [[CrossRef](#)]
35. Chen, Z.; Xie, Y.; Liu, J.; Shen, L.; Cheng, X.; Han, H.; Yang, M.; Shen, Y.; Zhao, T.; Hu, J. Distinct seasonality in vertical variations of tropospheric ozone over coastal regions of southern China. *Sci. Total Environ.* **2023**, *874*, 162423. [[CrossRef](#)]
36. Liu, J.J.; Jones, D.B.; Worden, J.R.; Noone, D.; Parrington, M.; Kar, J. Analysis of the summertime buildup of tropospheric ozone abundances over the Middle East and North Africa as observed by the Tropospheric Emission Spectrometer instrument. *J. Geophys. Res. Atmos.* **2009**, *114*, D05304. [[CrossRef](#)]
37. Liu, Y.; Liu, J.; Xie, M.; Fang, K.; Tarasick, D.W.; Wang, H.; Meng, L.; Cheng, X.; Han, H.; Zhang, X. ENSO teleconnection to interannual variability in carbon monoxide over the North Atlantic European region in spring. *Front. Environ. Sci.* **2022**, *10*, 1027. [[CrossRef](#)]
38. Lin, J.; McElroy, M.B. Impacts of boundary layer mixing on pollutant vertical profiles in the lower troposphere: Implications to satellite remote sensing. *Atmos. Environ.* **2010**, *44*, 1726–1739.

39. Keller, C.A.; Long, M.S.; Yantosca, R.M.; Da Silva, A.; Pawson, S.; Jacob, D.J. HEMCO v1. 0: A versatile, ESMF-compliant component for calculating emissions in atmospheric models. *Geosci. Model Dev.* **2014**, *7*, 1409–1417. [[CrossRef](#)]
40. Guenther, A.; Jiang, X.; Heald, C.L.; Sakulyanontvittaya, T.; Duhl, T.a.; Emmons, L.; Wang, X. The model of emissions of gases and aerosols from nature version 2.1 (MEGAN2. 1): An extended and updated framework for modeling biogenic emissions. *Geosci. Model Dev.* **2012**, *5*, 1471–1492. [[CrossRef](#)]
41. Hudman, R.C.; Moore, N.E.; Mebust, A.K.; Martin, R.V.; Russell, A.R.; Valin, L.C.; Cohen, R.C. Steps towards a mechanistic model of global soil nitric oxide emissions: Implementation and space based-constraints. *Atmos. Chem. Phys.* **2012**, *12*, 7779–7795. [[CrossRef](#)]
42. Hoesly, R.M.; Smith, S.J.; Feng, L.; Klimont, Z.; Janssens-Maenhout, G.; Pitkanen, T.; Seibert, J.J.; Vu, L.; Andres, R.J.; Bolt, R.M. Historical (1750–2014) anthropogenic emissions of reactive gases and aerosols from the Community Emissions Data System (CEDS). *Geosci. Model Dev.* **2018**, *11*, 369–408. [[CrossRef](#)]
43. Van der Werf, G.R.; Randerson, J.T.; Giglio, L.; Collatz, G.; Mu, M.; Kasibhatla, P.S.; Morton, D.C.; DeFries, R.; Jin, Y.v.; van Leeuwen, T.T. Global fire emissions and the contribution of deforestation, savanna, forest, agricultural, and peat fires (1997–2009). *Atmos. Chem. Phys.* **2010**, *10*, 11707–11735. [[CrossRef](#)]
44. Gong, C.; Liao, H. A typical weather pattern for ozone pollution events in North China. *Atmos. Chem. Phys.* **2019**, *19*, 13725–13740. [[CrossRef](#)]
45. Ambade, B.; Sankar, T.K.; Kumar, A.; Sethi, S.S. Characterization of PAHs and n-Alkanes in atmospheric aerosol of Jamshedpur city, India. *J. Hazard. Toxic Radioact. Waste* **2020**, *24*, 04020003. [[CrossRef](#)]
46. Hussain, A.J.; Sankar, T.K.; Vithanage, M.; Ambade, B.; Gautam, S. Black Carbon emissions from traffic contribute sustainability to air pollution in urban cities of India. *Water Air Soil Pollut.* **2023**, *234*, 217. [[CrossRef](#)]
47. Ambade, B. Characterization of PM10 over urban and rural sites of Rajnandgaon, central India. *Nat. Hazard.* **2015**, *80*, 589–604. [[CrossRef](#)]
48. Lv, M.; Li, Z.; Jiang, Q.; Chen, T.; Wang, Y.; Hu, A.; Cribb, M.; Cai, A. Contrasting trends of surface PM<sub>2.5</sub>, O<sub>3</sub>, and NO<sub>2</sub> and their relationships with meteorological parameters in typical coastal and inland cities in the Yangtze River Delta. *Int. J. Environ. Res. Public Health* **2021**, *18*, 12471. [[CrossRef](#)] [[PubMed](#)]

**Disclaimer/Publisher’s Note:** The statements, opinions and data contained in all publications are solely those of the individual author(s) and contributor(s) and not of MDPI and/or the editor(s). MDPI and/or the editor(s) disclaim responsibility for any injury to people or property resulting from any ideas, methods, instructions or products referred to in the content.